

Local Patch Classification Based Framework for Single Image Super-Resolution

Yang Zhao, *Member, IEEE*, Ronggang Wang, *Member, IEEE*, Wei Jia, *Member, IEEE*, Jianchao Yang, Wenmin Wang *and* Wen Gao, *Fellow, IEEE*

Abstract—Recent learning-based super-resolution (SR) methods often focus on the dictionary learning or network training. In this paper, we detailedly discuss a new SR framework based on local classification instead of traditional dictionary learning. The proposed efficient and extendible SR framework is named as local patch classification (LPC) based framework. The LPC framework consists of a learning stage and a reconstructing stage. In the learning stage, image patches are classified into different classes by means of the proposed local patch encoding (LPE), and then a projection matrix is computed for each class by utilizing a simple constraint. In the reconstructing stage, an input LR patch can be simply reconstructed by computing its LPE code and then multiplying corresponding projection matrix. Furthermore, we establish the relationship between the proposed method and the anchored neighborhood regression based methods; and we also analyze the extendibility of the proposed framework. The experimental results on several image sets demonstrate the effectiveness of the proposed framework.

Index Terms—Single-image super-resolution, upsampling, local binary pattern

I. INTRODUCTION

SINGLE image super-resolution (SR), also known as image upsampling or image upscaling, is a fundamental technique for various applications in machine vision and image processing, such as digital photographs, image editing, high-definition television and ultra-high-definition television, medical image processing, object recognition, and recent face hallucination [58]. The goal of image SR is to recover a high-resolution image (HRI) from a low-resolution image (LRI). How to reconstruct high quality HRI with low cost is still a challenging task.

One basic type of SR method is the interpolation-based

algorithm, such as nearest neighbor, bilinear interpolation, bicubic interpolation, and splines [1-2]. Unfortunately, these methods often produce unnatural artifacts, such as blurring, ringing, and jagged edges. Thus many interpolation based methods have been proposed to suppress the unnatural artifacts by means of edge prior knowledge [3-5], different interpolating grids [6-8], and edge sharpening processes [9-11], etc. These improved methods are able to refine the sharpness of edges, but cannot recover high-frequency details.

Another classic type of SR method is the reconstruction-based method, which imposes the similarity constraint between the downsampling of the reconstructed HRI and the original LRI. Early multi-frame reconstruction based methods [12] fused multiple LRIs of the same scene to recover an HRI. However, the multiple frames were difficult to align and tended to produce extra artifacts. Recently, many single-image reconstruction based methods have been proposed by means of various image models or constraints, such as, gradient constraints [13-17], local texture constraint [22], total variation regularizer [23], steering kernel regression based constraint [21], and de-blurring based methods [18-20]. However, the performance of these reconstruction based algorithms degrades rapidly when the magnification factor becomes very large.

To recover missing details, many example-based or learning-based SR methods have been proposed over the years. Generally, the example-based methods aim to learn the missing high-frequency information from the low-resolution (LR) /high-resolution (HR) example pairs. This type of method is first proposed in [24] and is further developed in [25-56]. Some typical kinds of learning based SR methods have been proposed, such as the neighbor embedding based methods [25-29], the sparse representation based methods [30-38], and the local self-exemplar based methods [39-43]. Although these example-based methods can recover fine details, the computational cost of these methods is quite high. Recently, some fast and high-performance models have been successfully applied in image SR scenario, e.g., the random forest based methods [50], the efficient anchor neighborhood regression (ANR) based methods [44-49], and the deep neural network based methods [51-56].

Generally, the target of learning based SR methods is to establish a mapping function from LR space to HR space. For example, traditional learning-based SR models often compute the mapping function by $\mathbf{x}_i = f(\mathbf{y}_i)$, where $\{\mathbf{x}\}_{i=1}^{N_S}$ and $\{\mathbf{y}\}_{i=1}^{N_S}$ denote the HR patches and the LR patches, respectively. The mapping function $f(\cdot)$ is needed to be calculated for each LR patch \mathbf{y}_i , and thus the total computation cost is often too high. To avoid the patch-by-patch optimization of the reconstruction

This work was partly supported by the grant of National Science Foundation of China 61402018, 61370115, 61305093, china 863 project of 2015AA015905, Shenzhen Peacock Plan JCYJ20150331100658943, and Guangdong Province Project 2014B010117007 for funding.

Y. Zhao and W. Jia are with the School of Computer and Information, Hefei University of Technology, 193 Tunxi Road, Hefei 230011, China (email: yzhao@hfut.edu.cn; icg.jiawei@gmail.com)

Y. Zhao, R. Wang, W. Wang, and W. Gao are with the School of Electronic and Computer Engineering, Peking University Shenzhen Graduate School, 2199 Lishui Road, Shenzhen 518055, China (email: zhaoyang@pkusz.edu.cn; rgwang@pkusz.edu.cn; wangwm@pkusz.edu.cn; wgao@pku.edu.cn)

J. Yang is with the Snapchat Inc, Venice, CA 90291, USA (email: jianchao.yang@snapchat.com)

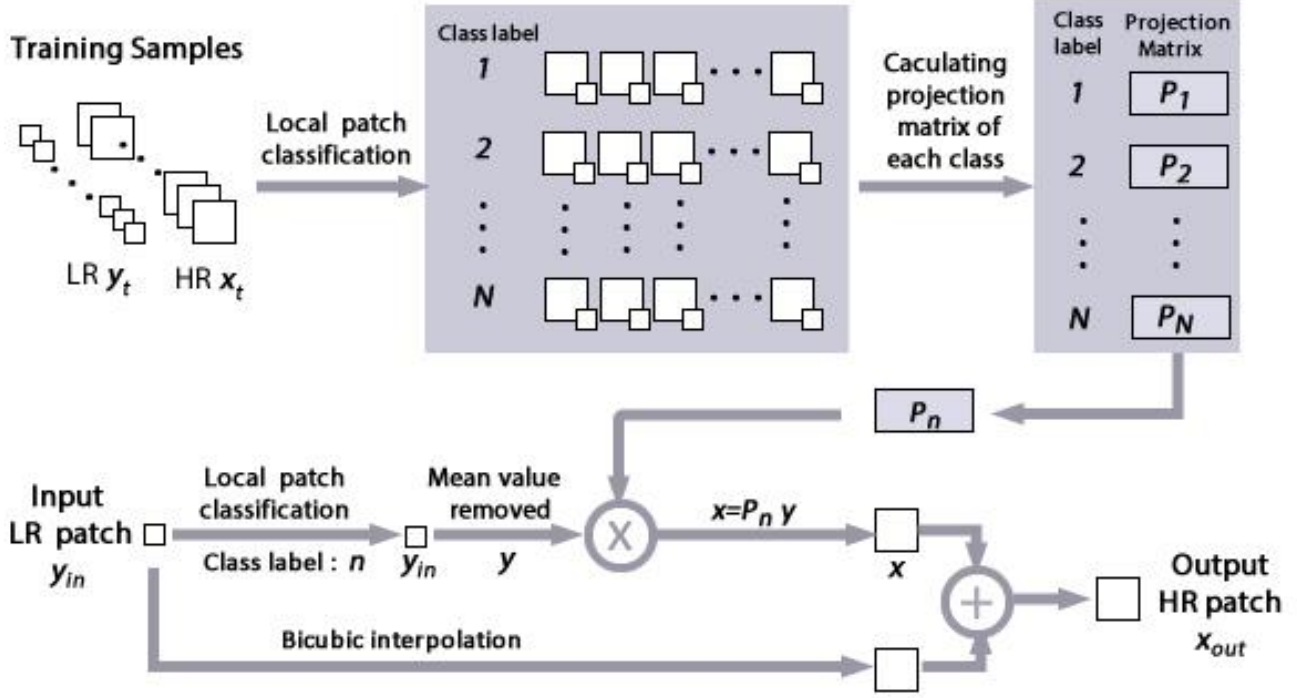


Fig. 1 The framework of the proposed method

weights or coefficients, Timofte *et al.* [44-45] introduced an efficient way to compute the $f(\cdot)$ by means of the dictionary atoms $\{\mathbf{d}_i\}_{i=1}^{N_d}$ and corresponding HR labels, i.e., $\mathbf{x}_i = f(\mathbf{d}_i)$. Then the mapping function $f(\mathbf{y}_i)$ of a LR input \mathbf{y}_i can be simply estimated by utilizing the pre-computed mapping $f(\mathbf{d}_i)$ of its nearest atom \mathbf{d}_i . Most recently, the convolutional networks are used to fit the mapping function, i.e., $\mathbf{X} = f(\mathbf{Y})$, where \mathbf{X} and \mathbf{Y} denote the HRI and LRI, separately. These end-to-end networks can directly reconstruct the entire image and also get rid of the complex patch-by-patch computation.

There are also other ways to avoid the patch-by-patch calculation of $f(\cdot)$. For example, if we can classify all the local patches into different classes $\{C\}_{n=1}^N$, we can setup the mapping of a class instead of individual patch, i.e., $\mathbf{x} = f(\mathbf{y} | \mathbf{y} \in C_n)$. To our best knowledge, recent state-of-the-art learning-based SR methods often focus on dictionary learning or network training, classification based SR framework has not been detailedly discussed. Is the classification based model effective for SR scenario? How to establish an efficient classification based SR framework? To answer these questions, this paper proposed a general and extendible SR framework, namely local patch classification (LPC) based framework. In the proposed framework, image patches are classified into different classes by means of local feature extraction methods, and then a projection matrix is computed for each class to characterize the projection relationship between the LR and HR patches. In the reconstruction stage of the proposed framework, an input LR patch can be simply reconstructed by calculating its class-label and then multiplying the corresponding embedding matrix. Furthermore, we propose a specific patches classification method based on local patch encoding (LPE) and

correspondingly present a simple constraint to calculate the projection matrix for each class of local patches. Experimental results demonstrate that the proposed framework can efficiently recover the HRIs.

Overall, the main technical contributions of this work are summarized as follows.

- 1) Traditional learning-based SR methods often focus on dictionary learning, while this paper try to discuss a new SR framework based on classification methods. The proposed framework is elastic and extendible. Hence, various local patch classification methods can be directly applied in the LPC framework. Moreover, we also analyse the relationship between the proposed SR framework and the efficient ANR methods [44-49].
- 2) For classifying the local patches, we propose a specific method, i.e., the LPE, to describe the local distribution. The LPE code can be directly used as the class-label and thus no dictionary needs to be pre-learned in the proposed method. Furthermore, the discrimination capability of LPE can be easily enhanced by directly increasing the bit-depth of LPE code.
- 3) Based on the accurate classification of local patches, we also present a simple way to compute the projection matrix by minimizing the total reconstruction errors of each class. Compared with the projection matrix calculated by means of the ridge regression, the proposed projection matrix can produce comparable or even better reconstruction results.

The following paragraphs of this paper are organized as follows. Section II presents the proposed method in detail. Section III gives the experimental results to testify the

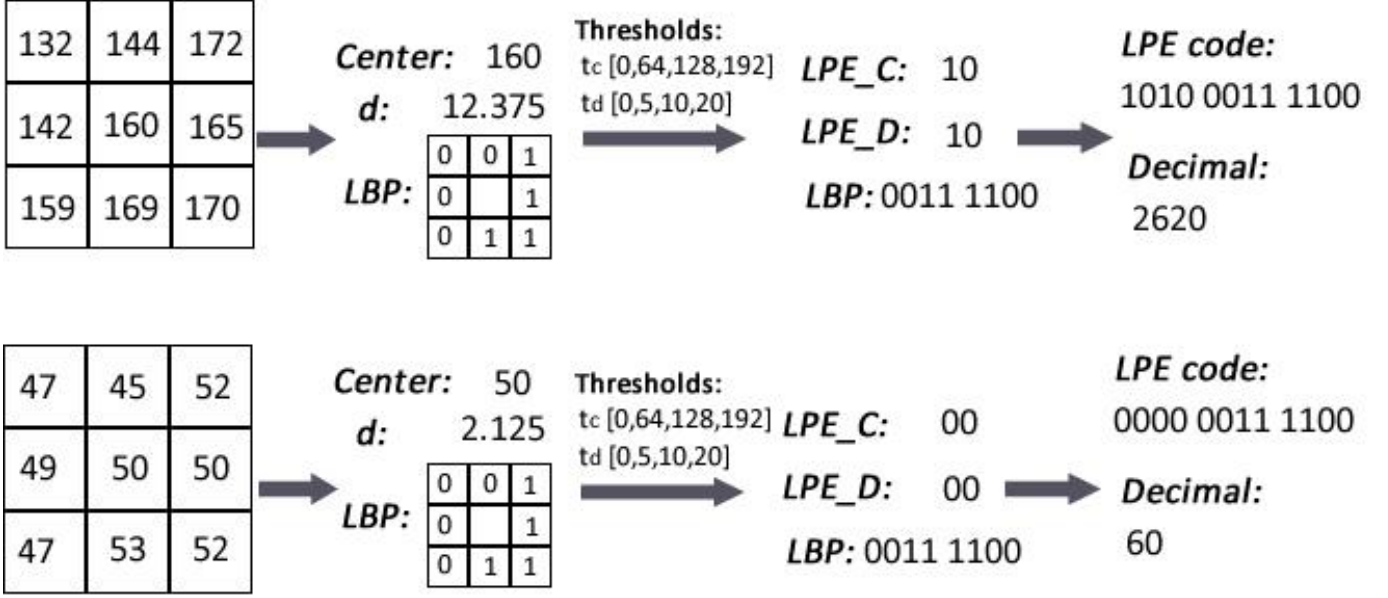


Fig.2 Illustration of the 12-bits LPE codes of two different patches

effectiveness of the proposed method, and Section V concludes the paper.

II. LOCAL PATCH CLASSIFICATION BASED SR METHOD

A. The Proposed SR Framework

As illustrated in Fig. 1, the proposed LPC based SR framework can be divided into two stages: a learning stage in which the local patches are classified into different classes and projection matrix is then calculated for each class; and a reconstructing stage in which LR input is reconstructed by means of corresponding pre-computed projection matrix.

In the learning stage, various LR patches and corresponding HR patches are randomly selected from training images. These LR and HR patch pairs are then classified into N classes by a local patch classification process. Hence, the patches in the same class have similar local pattern and grayscale distribution. Finally, a projection matrix is computed for each class to represent the mapping relationship between the LR patches and the HR patches.

In the reconstructing stage, the class-label n of the input LR patch is firstly calculated. The input patch is then multiplied with the corresponding pre-computed projection matrix P_n to produce its HR patch. It should be noticed that, in practice, the training patches and input patches are mean-value-removed as in many other learning-based SR methods, e.g., [30, 31, 44, 45]. That means the traditional interpolation-based methods are used to obtain an initial patch and the learning-based processes are mainly to recover the missing high-frequency components. Hence, the reconstructed HR patch is finally combined with the bicubic-interpolated patch to obtain the HR output.

In the following, we firstly introduce an efficient local patches classification method and then present a simple constraint to calculate the projection matrix. At last, we further analyze the extendibility of the proposed framework.

B. Local Patch Encoding Based Patch Classification

In the proposed framework, patches with similar local distribution shall be classified into the same class. Therefore, we propose a LPE method based on a popular local descriptor of local binary pattern (LBP) [59]. The LBP code has been widely utilized to characterize the local pattern in many texture analysis works. Usually, the LBP coding strategy is described as follows.

$$LBP = \sum_{p=1}^{N_p} s(g_p - g_c) 2^{p-1}, \quad s(x) = \begin{cases} 1, & x \geq 0 \\ 0, & x < 0 \end{cases} \quad (1)$$

where g_c represents the gray value of the central pixel and g_p ($p = 1, 2, \dots, N_p$) denotes the gray value of the neighboring pixels around the central pixel, and N_p is the total number of neighboring pixels. However, traditional LBP merely characterizes the local structure, but omits to describe the local grayscales [60-61]. Hence, we propose a simple but effective local patch encoding method to distinguish different local patches via their binary structure and local gray value difference.

The gray value of central pixel represents the grayscale level of the local patch. Hence we quantize the central pixel value into various levels by means of a LPE code of central pixel value (LPE_C), which is defined as,

$$LPE_C = \text{bin}(Q_{c_i} | g_c \in Q_{c_i}), i = (1, 2, \dots, 2^{N_c}) \quad (2)$$

where Q_{c_i} ($i = 1, 2, \dots, 2^{N_c}$) is the index of gray value interval quantized by a series of quantization thresholds, N_c denotes the bit-depth of the central pixel value encoding, and $\text{bin}(\cdot)$ denotes binarization process. The LPE_C code thus denotes the binary index of the quantized interval covering the central gray value. For example, if N_c is set as 2, the central gray value is

quantized into four intervals and the binary indexes of these four intervals are “00”, “01”, “10”, and “11”, respectively. In this paper, we utilize a series of homogeneous thresholds t_c to quantize the central pixel value, and the thresholds t_c is simply set as $[0, \frac{256}{N_c}, \frac{256}{N_c} \times 2, \dots, \frac{256}{N_c} \times (N_c - 1)]$.

The mean local gray value difference is utilized to describe the magnitude of gray value difference, which is computed as,

$$d = \frac{1}{N_p} \sum_{p=1}^{N_p} |g_p - g_c| \quad (3)$$

where g_p , g_c and N_p have been defined in Eqn.(1). The mean local gray value difference d can also be quantized into several levels by a set of thresholds. As a result, the LPE code of local difference (LPE_D) is defined as,

$$LPE_D = \text{bin}(Q_{d_j} | d \in Q_{d_j}), j = (1, 2, \dots, 2^{N_d}) \quad (4)$$

where Q_{d_j} ($j = 1, 2, \dots, 2^{N_d}$) denotes the index of quantized interval of local gray value difference, N_d is the bit-depth of the local gray value difference encoding, and $\text{bin}(\cdot)$ denotes binarization process. The LPE_D code denotes the binary index of the interval covering the mean local gray value difference d . In this paper, the thresholds t_d used to quantize the local gray value difference are experimentally set as $[0, 5, 10, \dots, 5 \times (N_d - 1)]$ respectively.

Finally, we obtain the LPE code of a local patch by the concatenation of the LPE_C code, the LPE_D code, and the LBP code:

$$LPE = \text{bin}(Q_{c_i} | g_c \in Q_{c_i}) \oplus \text{bin}(Q_{d_j} | d \in Q_{d_j}) \oplus \text{bin}(\sum_{p=1}^{N_p} s(g_p - g_c) 2^{p-1}) \quad (5)$$

where \oplus denotes the concatenation of binary codes.

In this work, we extract the LPE code from a 3×3 LR patch, and N_p is thus set as 8. After local patch encoding process, each LR patch is encoded by a LPE code with the bit-depth of $(N_c + N_d + N_p)$, and this LPE code can be regarded as the class-label of the LR patch and its corresponding HR patch. Note that the minimum bit-depth is 8, and in this case, the 8-bit LPE code is set as the traditional LBP code. When the bit-depth of LPE code increases, we alternately increase the quantization levels of LPE_C and LPE_D. For example, the 12-bit LPE code is the concatenation of 2-bit LPE_C code, 2-bit LPE_D code, and 8-bit LBP code. Fig.2 illustrates the detailed calculation of 12-bit LPE codes of two local patches.

Note that there are many local patch classification methods, the reasons why we merely utilize the simple LPE encoding in this paper are listed as follows. Firstly, the proposed encoding process is easy to be calculated. Secondly, the LPE code of a local patch can be directly used as its class-label and therefore the complex dictionary learning process or extra classifier can be omitted. For example, if a patch is encoded as “0000 0011 1100” (60), this patch can be directly classified into the 60-th class. Thirdly, motivated by efficient LBP-variants used in local texture analysis works [60-61], the simple local encoding process can accurately characterizes the local distribution by

Algorithm 1. Learning stage of the LPC based SR

- 1) **Input:** LR samples and corresponding HR samples
 - 2) **Classification:**
Classify LR and HR samples into total N classes by means of the LPE codes computed by Eqn.(5)
 - 3) **for** each class n of N do
 - a) Randomly select N_o LR and HR samples from the n -th class;
 - b) Removed the mean patch value from each LR and HR sample;
 - c) Calculate the projection matrix \mathbf{P}_n by means of Eqn.(7).
 - 4) **end for**
 - 5) **Outputs:** \mathbf{P}_n ($n = 1, 2, \dots, N$) for each class.
-

Algorithm 2. Reconstruction stage of the LPC based SR

- 1) **Inputs:** LR image \mathbf{Y} , magnified factor s , projection matrix \mathbf{P}_n ($n = 1, 2, \dots, N$)
 - 2) **Initialization:** set the HR image $\mathbf{X} = 0$
 - 3) **for** each image patch \mathbf{y}_{in} in \mathbf{Y} do
 - a) Upsample \mathbf{y}_{in} by using bicubic interpolation with a factor of s ;
 - b) Remove the mean value from \mathbf{y}_{in} to get \mathbf{y} ;
 - c) Obtain the class-label n of \mathbf{y}_{in} by computing its LPE code with Eqn.(5);
 - d) Reconstruct the HR output \mathbf{x}_{out} by means of Eqn.(9);
 - e) Add \mathbf{x}_{out} to the corresponding pixels in \mathbf{X} .
 - 4) **end for**
 - 5) **Average** overlapping regions of \mathbf{X} between the adjacent patches
 - 6) **Outputs:** HR image \mathbf{X} .
-

encoding the gray value level, local gray value difference and local textural structure. Furthermore, the proposed LPE have better discriminative capability than the traditional LBP. As shown in Fig.2, two different patches may have the same LBP code, while the proposed LPE can easily distinguish them. Lastly, the patches can be accurately classified into more classes by simply increasing the bit-depth of LPE code, while the computation complexity of the reconstructing stage is almost not increased.

C. Derivation of Projection Matrix

In the proposed SR framework, local patches are classified into various classes according to their LPE codes. A projection matrix is then computed for each class to establish the mapping relationship between LR patches and HR patches. One basic constraint of image SR is that the upsampled LR patch should be consistent with its HR patch. Hence, we propose to calculate the projection matrix by minimizing the total reconstruction errors in one class. This constraint can be described as,

$$\min_{\mathbf{P}} \sum_{i=1}^{N_o} \|\mathbf{P}\mathbf{y}_i - \mathbf{x}_i\|_2^2 \quad (6)$$

where \mathbf{y}_i denotes a LR patch, \mathbf{x}_i is its corresponding HR patch, \mathbf{P} is the projection matrix, and N_o denotes the number of

training patches in this class. It should be noticed that the patches \mathbf{y}_i and \mathbf{x}_i are in the form of vectors. The algebraic solution of Eqn.(6) is given by,

$$\mathbf{P} = \sum_{i=1}^{N_o} \mathbf{x}_i \mathbf{y}_i^T (\sum_{i=1}^{N_o} \mathbf{y}_i \mathbf{y}_i^T)^{-1} \quad (7)$$

where the inverse of matrix denotes the generalized inverse.

In this paper, we randomly select N_o (LR and HR) patch pairs from each class to compute its projection matrix. Note that the proposed constraint is based on the assumption that local patches are accurately classified. If the patches in one class have different local distributions, it is unreasonable to reconstruct them with one same projection matrix. Vice versa, more accurate patches classification results can further enhance the performance of the proposed projection matrix. Hence, this constraint is very suitable for the proposed SR framework, which is based on accurate local patch classification.

In the reconstructing stage, a LR patch \mathbf{y} with class-label n can be simply reconstructed as follows,

$$\mathbf{x} = \mathbf{P}_n \mathbf{y} \quad (8)$$

where \mathbf{P}_n denotes the projection matrix of the n -th class. In practice, the \mathbf{y} is obtained by subtracting the mean value from the LR input \mathbf{y}_{in} . Therefore, the final HR output \mathbf{x}_{out} is the summation of the reconstructed HR patch \mathbf{x} and the bicubic-interpolated LR input:

$$\mathbf{x}_{out} = \mathbf{P}_n \mathbf{y} + H^T U \mathbf{y}_{in} \quad (9)$$

where \mathbf{y} denotes the mean-value-removed LR input, U denote an upsampling operator, and H is a blurring operator.

The proposed algorithms for the learning stage and the reconstructing stage are summarized in **Algorithm 1** and **Algorithm 2**, respectively.

D. Extendibility of the Proposed SR Framework

In the following we firstly clarify the relationship between the ANR model and the LPC model. The extendibility of the proposed SR framework is then analyzed.

In the ANR based methods [44-49], the nearest neighbor atom of a LR input \mathbf{y} is firstly searched from the learned dictionary. The pre-computed projection matrix of this atom is then used to estimate the projection matrix of \mathbf{y} . If we view each dictionary atom as a class-center, the ANR based methods also roughly classify the input patches into different classes according to the distances between \mathbf{y} and each class-center. Therefore, the dictionary learning process in the ANR can also be viewed as a special local classification process.

The proposed SR framework can be easily extended to various methods¹. Firstly, various local features and local classification methods can be applied in the local patch classification process, such as gradient based features, variants of LBP features, filter based features, and even deep neural network. Secondly, if we view the dictionary learning process as a special local classification method and use the dictionary atoms as the class-labels, different dictionary learning methods

can also be utilized in the learning stage, such as K-means clustering, neighbor embedding based methods, sparse representation based methods, and so on.

Thirdly, different constraints can be utilized to compute the projection matrix for each class. For example, the ANR applied a constraint that minimizes the representation error of the dictionary atom. In the ANR based methods, the ridge regression is used to calculate the representation of LR input feature \mathbf{y} as follows,

$$\min_{\alpha} \|\mathbf{y} - \mathbf{N}_l \alpha\|_2^2 + \lambda \|\alpha\|_2 \quad (10)$$

where \mathbf{N}_l denotes the neighborhood in LR space, and λ is a weighting factor to stabilize the solution. The algebraic solution of Eqn. (10) is given by

$$\alpha = (\mathbf{N}_l^T \mathbf{N}_l + \lambda \mathbf{I})^{-1} \mathbf{N}_l^T \mathbf{y} \quad (11)$$

As a result, the HR patch can be estimated by the same coefficients α :

$$\mathbf{x} = \mathbf{N}_h \alpha = \mathbf{N}_h (\mathbf{N}_l^T \mathbf{N}_l + \lambda \mathbf{I})^{-1} \mathbf{N}_l^T \mathbf{y} \quad (12)$$

where \mathbf{N}_h is the HR neighborhood corresponding to \mathbf{N}_l . The projection matrix is then defined by

$$\mathbf{P}_2 = \mathbf{N}_h (\mathbf{N}_l^T \mathbf{N}_l + \lambda \mathbf{I})^{-1} \mathbf{N}_l^T \quad (13)$$

Note that the l_2 norm is utilized in both Eqn. (6) and Eqn. (10), so that the projection matrixes can be easily calculated by means of their close-form solutions. In this paper, we adopt both the projection matrix \mathbf{P}_1 computed by Eqn. (7) and the projection matrix \mathbf{P}_2 computed with the traditional ridge regression. The LPC based SR method with the projection matrix \mathbf{P}_1 is denoted by ‘‘LPCxxbits_P1’’; the LPC based SR method with the projection matrix \mathbf{P}_2 is denoted by ‘‘LPCxxbits_P2’’; and where the ‘‘xxbits’’ denotes the bit-depth of the LPE code.

III. EXPERIMENTS

A. Testing Image Sets

We test the proposed method on three testing image sets, i.e., ‘‘Set 5’’, ‘‘Set 14’’, and ‘‘B100’’. ‘‘Set 5’’ [28] and ‘‘Set 14’’ [36] contain 5 and 14 commonly used images respectively for SR evaluation. ‘‘B100’’ [44] consists of 100 testing images selected from the Berkeley image dataset [57]. For color image, it is firstly converted from RGB to YUV. Various SR methods are then applied only on Y (intensity) component, and bicubic interpolation is used for U and V components. In our experiments, the input LRIs are obtained by downsampling the original HRIs with bicubic interpolation and the LRIs are then upsampled to their original size with different methods. Note that the ASDS [32] method firstly filtered and then downsampled the HRIs to obtain the LRIs, which is slightly different to other methods. The upsampling factors in our experiment are set as 2, 3, and 4 respectively.

¹ The extendable code of the proposed method can be downloaded from: <http://yzhaoev.weebly.com/projectpage/lpcsr.html>

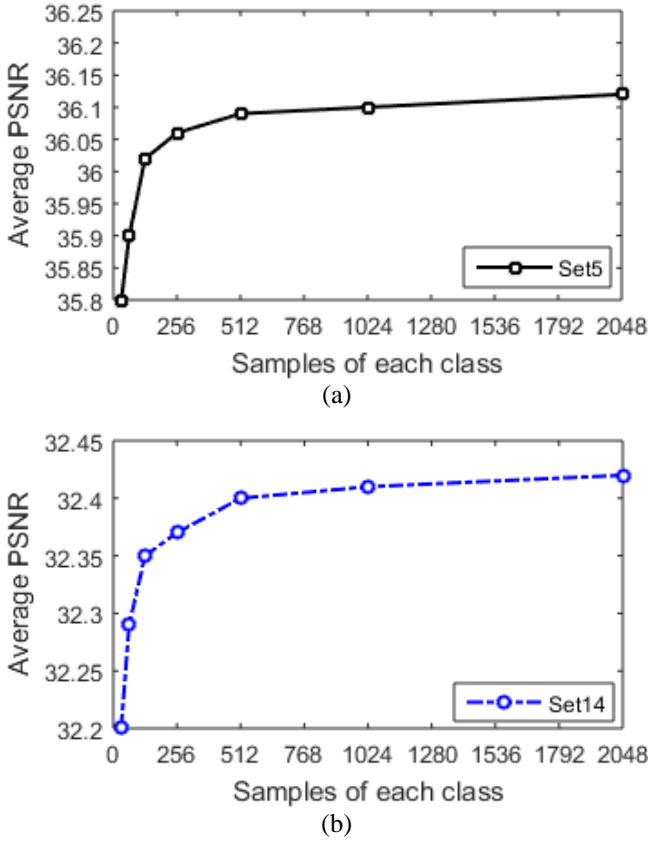


Fig. 3 Average PSNR (dB) of 2 \times magnification with different numbers of selected samples in each class, (a) on image set ‘Set5’, (b) on image set ‘Set14’.

B. Compared Methods and Implementation Details

In this paper, the proposed method is compared with many typical learning-based SR methods, such as the LLE [27], the ScSR [30], the Zeyde’s method [36], the ASDS [32], the ANR

[44], and the A+ [45]. In addition, we also use some new state-of-the-art SR methods as further comparison, such as convolutional neural network (CNN) based methods [52–53].

For calculating the LPE codes in the patches classification process, we select various sets of thresholds to quantize the central gray value and the mean local gray value difference. We experimentally select the two sets of thresholds as in part B of Section II, which achieve the highest average PSNR values on ‘Set5’ and ‘Set14’. For calculating the projection matrix with Eqn. (13), we use the same factor λ as in [44].

We used the same training set proposed by Yang *et al.* [30], which is also used in many other methods. Fig. 3 illustrates the average PSNR values on ‘Set5’ and ‘Set14’ with different numbers of patches that used to calculate the projection matrix in each class. We can find that more samples always obtain better results. Hence we randomly select 2048 LR and HR patch pairs from each class. Note that the training set only contains 91 images and thus the total numbers of patches may be less than 2048 in some classes. On this condition, we used all the patches in one class to compute its projection matrix.

C. Experimental Details

Fig. 4 illustrates SR results of ‘monarch’ image with different methods for 2 \times magnification. By comparing the edges, we can get the following observations. Firstly, the bicubic interpolation produces blurry edges and these learning-based methods can recover sharp edges. Secondly, the A+, the LPC12bits_P₁, and the LPC12bits_P₂ recover sharper edges than other methods. Thirdly, by comparing the tiny edge area which is marked in the red rectangle, the proposed LPC based methods can reproduce better result than the state-of-the-art A+. Lastly, the LPC based methods with two kinds of projection matrixes reproduce very similar results. Furthermore, the residual component between each SR result and the ground truth HRI is also illustrated in the blue square. By comparing different residual maps, it can be found that the

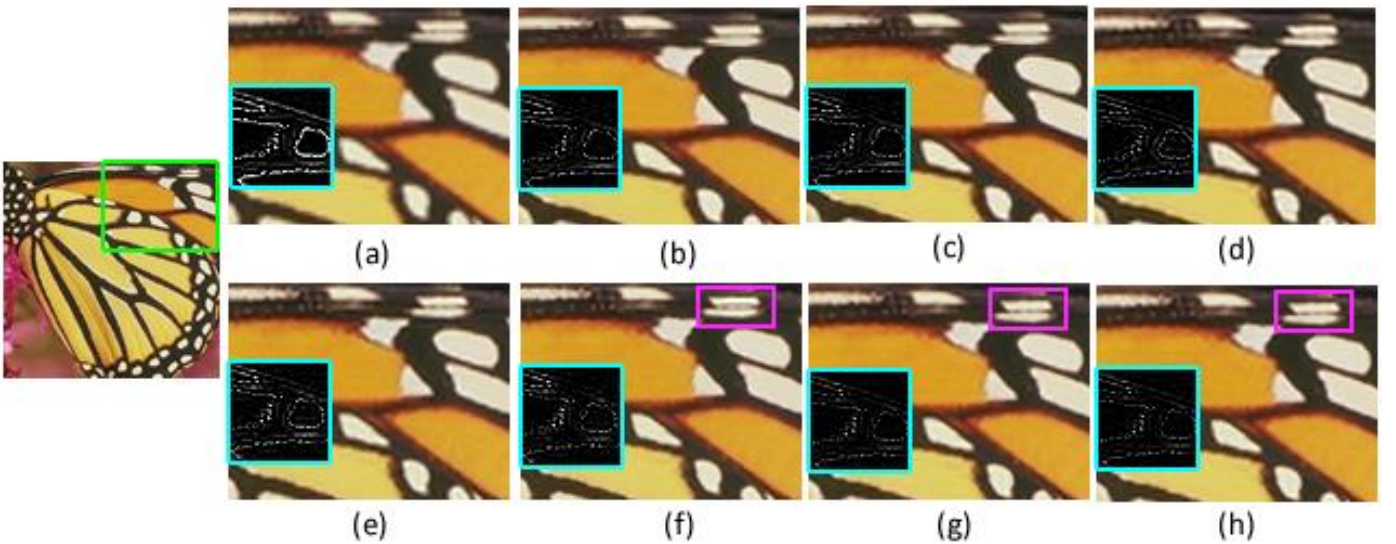


Fig. 4. SR results of ‘monarch’ image with different methods (2 \times), (a) with bicubic interpolation, (b) with the LLE [27], (c) with the ScSR [30], (d) with the ASDS [32], (e) with the ANR [44], (f) with the A+ [45], (g) with the LPC12bits_P₁, (h) with the LPC12bits_P₂. The selected area in the blue square show the residual map between each result and ground truth.

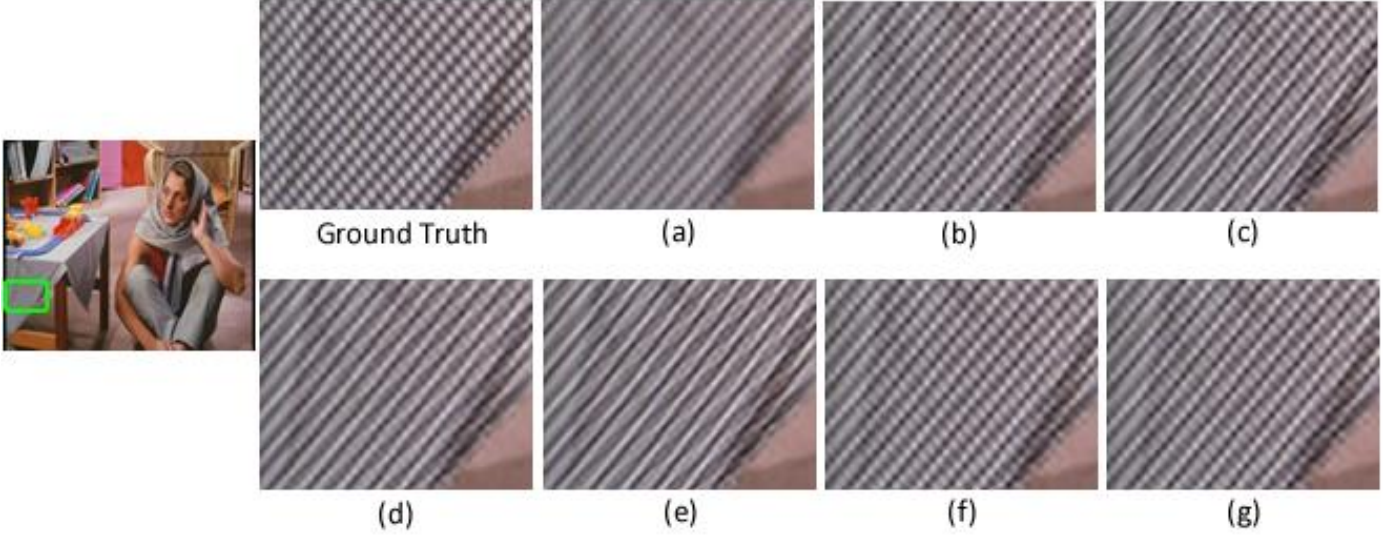


Fig.5. SR results of “barbara” image with different methods ($3\times$), (a) with bicubic interpolation, (b) with the ScSR [30], (c) with the ASDS [32], (d) with the ANR [44], (e) with the A+ [45], (g) with the LPC12bits_P₁, (h) with the LPC12bits_P₂.

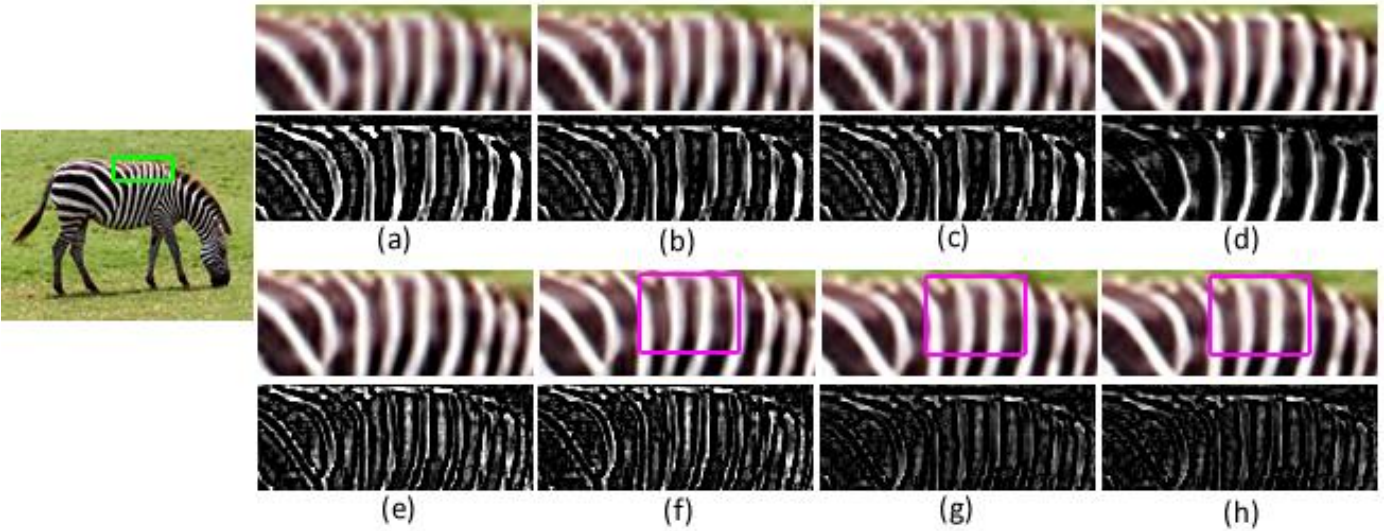


Fig.6. SR results of “zebra” image with different methods ($4\times$), (a) with bicubic interpolation, (b) with the LLE [27], (c) with the ScSR [30], (d) with the ASDS [32], (e) with the ANR [44], (f) with the A+ [45], (g) with the LPC12bits_P₁, (h) with the LPC12bits_P₂. The residual map between each SR result and ground truth is also given.

proposed LPC methods can produce lower difference to the ground truth image than other methods.

Fig.5 shows $3\times$ magnification results of “barbara” image with different methods. By comparing the texture area, we can find that the ASDS, the ANR, and the A+ obviously sharpen and damage the original texture. This demonstrate that these methods can effectively recover sharp edges, but they may not reproduce natural texture. Owing to the accurate local pattern description, the proposed LPC based methods can maintain the local textural structure and avoid over-sharpening of the texture along with sharpening of the edges. Hence, the proposed method can reconstruct clear and vivid texture.

Fig. 6 illustrates SR results of “zebra” image for $4\times$ magnification with these methods. By comparing the boundaries of streaks, we can get some similar findings to Fig.4.

First, the A+, the LPC12bits_P₁, and the LPC12bits_P₂ can reconstruct sharper edges than other methods. Second, by comparing the edge details marked in the red rectangle, the proposed LPC based methods can obtain sharper edges than the A+ for $4\times$ magnification. Last, by comparing the residual maps of different methods, the LPC based methods still have the least difference to the HRI.

Table I, Table II, and Table III list the objective assessment of $2\times$, $3\times$, and $4\times$ magnification on three image datasets of “Set5”, “Set14”, and “B100”, respectively. Two commonly used quantitative evaluation metrics PSNR and SSIM [62] are also adopted in this paper. However, the PSNR and SSIM cannot reflect image subjective quality well [42]. In [63], Yang *et al.* have observed that the information fidelity criterion (IFC) [64] index has the highest correlation with perceptual scores for

TABLE I. AVERAGE PSNR (dB), SSIM, AND IFC OF DIFFERENT METHODS ON IMAGE SET “Set5”

	2X			3X			4X		
	PSNR	SSIM	IFC	PSNR	SSIM	IFC	PSNR	SSIM	IFC
<i>Bicubic</i>	33.66	0.9383	5.72	30.40	0.8804	3.44	28.44	0.8250	2.29
<i>LLE</i>	35.57	0.9543	6.08	31.73	0.8836	4.24	29.64	0.8510	2.93
<i>ScSR</i>	35.38	0.9564	7.00	31.23	0.9068	4.15	29.43	0.8551	2.69
<i>ASDS</i>	34.85	0.9544	6.81	31.02	0.9003	4.31	29.54	0.8497	2.75
<i>Zeyde</i>	35.64	0.9559	6.87	31.79	0.9032	4.37	29.69	0.8533	2.70
<i>ANR</i>	35.82	0.9568	7.30	31.84	0.9072	4.39	29.68	0.8558	3.00
<i>LPC10bits</i> P_2	36.12	0.9573	7.31	32.22	0.9132	4.44	30.03	0.8729	3.11
<i>LPC10bits</i> P_1	36.10	0.9572	7.30	32.27	0.9125	4.40	30.09	0.8720	3.09
<i>LPC12bits</i> P_2	<u>36.14</u>	0.9585	<u>7.37</u>	<u>32.33</u>	0.9165	<u>4.49</u>	<u>30.19</u>	<u>0.8764</u>	3.19
<i>LPC12bits</i> P_1	36.19	<u>0.9582</u>	7.39	32.41	<u>0.9161</u>	4.57	30.22	0.8773	<u>3.13</u>

TABLE II. AVERAGE PSNR (dB), SSIM, AND IFC OF DIFFERENT METHODS ON IMAGE SET “Set14”

	2X			3X			4X		
	PSNR	SSIM	IFC	PSNR	SSIM	IFC	PSNR	SSIM	IFC
<i>Bicubic</i>	30.36	0.9417	5.83	27.67	0.8596	3.41	26.12	0.7857	2.27
<i>LLE</i>	31.91	0.9587	6.08	28.74	0.8836	3.89	26.95	0.8137	2.21
<i>ScSR</i>	31.21	0.9620	6.22	28.01	0.8882	4.04	26.57	0.8183	2.65
<i>ASDS</i>	31.15	0.9627	6.61	27.91	0.8938	4.11	26.94	0.8190	2.35
<i>Zeyde</i>	31.96	0.9589	6.25	28.80	0.8841	4.02	26.99	0.8159	2.67
<i>ANR</i>	31.95	0.9626	6.36	28.80	0.8890	3.67	27.00	0.8194	2.48
<i>A+</i>	32.39	0.9641	6.54	29.12	0.8940	4.04	27.34	0.8294	2.62
<i>LPC10bits</i> P_2	32.35	0.9677	6.86	29.11	0.9013	4.09	27.33	0.8398	2.69
<i>LPC10bits</i> P_1	32.39	0.9674	6.82	29.15	0.9016	4.13	27.35	0.8379	2.71
<i>LPC12bits</i> P_2	<u>32.44</u>	<u>0.9688</u>	7.27	<u>29.19</u>	<u>0.9088</u>	<u>4.22</u>	<u>27.40</u>	0.8603	2.87
<i>LPC12bits</i> P_1	32.47	0.9692	7.27	29.21	0.9093	4.23	27.42	<u>0.8596</u>	<u>2.84</u>

TABLE III. AVERAGE PSNR (dB), SSIM, AND IFC OF DIFFERENT METHODS ON IMAGE SET “B100”

	2X			3X			4X		
	PSNR	SSIM	IFC	PSNR	SSIM	IFC	PSNR	SSIM	IFC
<i>Bicubic</i>	29.35	0.8334	5.85	27.17	0.7361	3.47	25.95	0.6671	2.29
<i>LLE</i>	30.40	0.8674	6.12	27.84	0.7687	3.95	26.47	0.6937	2.74
<i>ScSR</i>	30.32	0.8709	6.24	27.74	0.7719	4.22	26.33	0.6997	2.85
<i>ASDS</i>	30.19	0.8712	6.72	27.65	0.7735	4.24	26.45	0.7003	2.97
<i>Zeyde</i>	30.40	0.8682	6.32	27.87	0.7693	4.18	26.51	0.6963	2.76
<i>ANR</i>	30.50	0.8706	6.59	27.90	0.7724	4.16	26.52	0.6991	2.67
<i>A+</i>	30.76	0.8762	6.64	28.18	0.7764	4.19	26.76	0.7062	2.72
<i>LPC10bits</i> P_2	30.74	0.8796	7.04	28.18	0.7885	4.20	26.80	0.7148	2.96
<i>LPC10bits</i> P_1	30.78	0.8792	7.06	28.20	0.7863	4.22	26.82	0.7151	2.90
<i>LPC12bits</i> P_2	<u>30.97</u>	<u>0.8825</u>	<u>7.12</u>	<u>28.26</u>	<u>0.7937</u>	4.34	<u>26.87</u>	<u>0.7223</u>	3.12
<i>LPC12bits</i> P_1	30.99	0.8827	7.14	28.27	0.7946	<u>4.32</u>	26.94	0.7223	<u>3.06</u>

TABLE IV. COMPARISON RESULTS WITH CNN BASED METHODS ON IMAGE SET “B100”

	2X			3X			4X		
	PSNR	SSIM	IFC	PSNR	SSIM	IFC	PSNR	SSIM	IFC
<i>Bicubic</i>	29.35	0.8334	5.85	27.17	0.7361	3.47	25.95	0.6671	2.29
<i>SRCNN</i>	31.06	0.8854	6.62	28.18	0.7780	4.14	26.79	0.7059	2.69
<i>VDSR</i>	31.30	0.8861	6.79	28.31	0.7789	4.24	26.93	0.7070	2.83
<i>LPC12bits</i> P_2	30.97	0.8825	7.12	28.26	0.7937	4.34	26.87	0.7223	3.12
<i>LPC12bits</i> P_1	30.99	0.8827	7.14	28.27	0.7946	4.32	26.94	0.7223	3.06
<i>LPC17bits</i> P_2	<u>31.26</u>	<u>0.8924</u>	<u>7.17</u>	<u>28.38</u>	0.7977	4.38	<u>26.99</u>	<u>0.7293</u>	3.18
<i>LPC17bits</i> P_1	31.24	0.8927	7.19	28.39	<u>0.7969</u>	<u>4.36</u>	27.06	0.7294	<u>3.11</u>

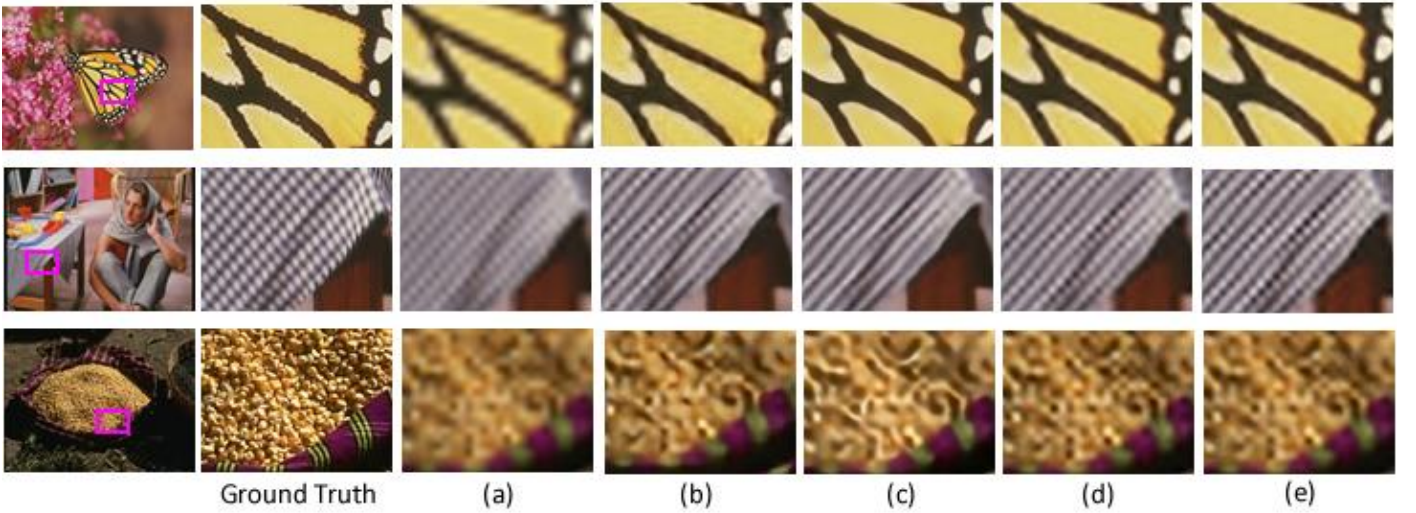


Fig. 7. SR results (4 \times) with different methods, (a) with bicubic interpolation, (b) with the SRCNN [52], (c) with the VDSR [53], (d) with the LPC12bits_P1, (e) with the LPC17bits_P1.

SR evaluation. Hence, the IFC index is also used in our experiment to verify the subjective quality of the SR results. We can get the following findings from these tables. First, the A+ and the proposed LPC based methods achieve better PSNR, SSIM, and IFC results than other methods. Second, the 10-bits LPC methods obtain comparable results with the A+, and the 12-bits LPC methods perform better than the A+. Third, the proposed methods always get much higher SSIM results than other methods. That demonstrates the results of LPC based method have better structure-similarity than these learning-based methods. Fourth, by comparing the average IFC indexes, the proposed methods still perform much better than other methods. Last, the proposed LPC methods with two kinds of projection matrixes obtain similar performance, which indicates different projection matrixes can be suitable for the proposed framework.

D. Comparison with recent CNN based SR methods

In recent years, several deep neural network methods have been successfully applied in SR scenario and have achieved impressive results. For example, Dong *et al.* [52] firstly proposed an effective CNN based SR method (SRCNN). Kim *et al.* [53] further trained a very deep CNN for SR (VDSR). In many CNN based methods [52-55], SR problem is treated as an end-to-end image reconstruction task. A convolutional network without pooling and fully connected layers are often utilized in these works. The CNN has a strong ability to fit high non-linear regression task, and thus the CNN based SR methods can obtain state-of-the-art results. Therefore, we further discuss the comparison with some current state-of-the-arts in this subsection.

Table IV lists the SR results of different methods on the largest test image set ‘B100’. By comparing the 12-bits LPC based methods with the SRCNN [52] and the VDSR [53], we can find that the VDSR gets higher average PSNR values than the LPC methods. However, the 12-bits LPC can achieve better SSIM and IFC results than the VDSR. When the depth of the LPE increases to 17 bits, the 17-bits LPC based methods outperform than the SRCNN and the VDSR. Note that the

SRCNN and the VDSR are also trained with the same training set [30]. The performance of the CNN based methods can be further improved by using more training images. In short, the proposed LPC based methods can achieve comparable objective quality with the state-of-the-art CNN based methods.

Comparing to traditional learning-based methods, the CNN based SR methods, e.g., the SRCNN and the VDSR, can reproduce much sharper edges, as illustrated in Fig. 7. However, the SRCNN and the VDSR also over-sharpen the texture area. That is probably because the edge-like patterns are relatively more stable than local texture, and thus the convolutional network can learn the edge details much better than the texture. In other words, the CNN based methods tend to sharpen images, while the proposed LPC is more faithful to the original image content. Hence, the CNN based methods obtain sharper and clearer results, and the LPC based methods are robust to both edge and texture by means of effective local classification.

E. Further analyses

The computational time of the proposed method depends on the image size. Given a LR input feature of size n and the pre-computed projection matrix of size $m \times n$, the complexity of local patch encoding is $O(n)$, and the complexity of multiplying the projection matrix with LR input is $O(m \times n)$. Hence, the overall complexity of the reconstructing process is $O(n)$. The complexities of the reconstruction stage of the proposed method and the ANR are at the same level.

As illustrated in Fig.8, we can find that better performance on ‘Set5’ and ‘Set14’ can be achieved when the bit-depth of LPE code increases. That is because the classification of local patches becomes more accurate when the bit-depth of LPE code increases. Although the computation cost of LPE process increases little when the bit-depth of LPE code increases, but much more projection matrixes have to be pre-computed. For example, 2^{12} (4096) projection matrixes are computed for 12-bit LPE code, and 2^{17} (131072) projection matrixes are required to be calculated for 17-bit LPE code. We thus mainly utilize the 12-bit LPE codes in the experiment to balance the quality of SR results and the number of pre-computed matrixes.

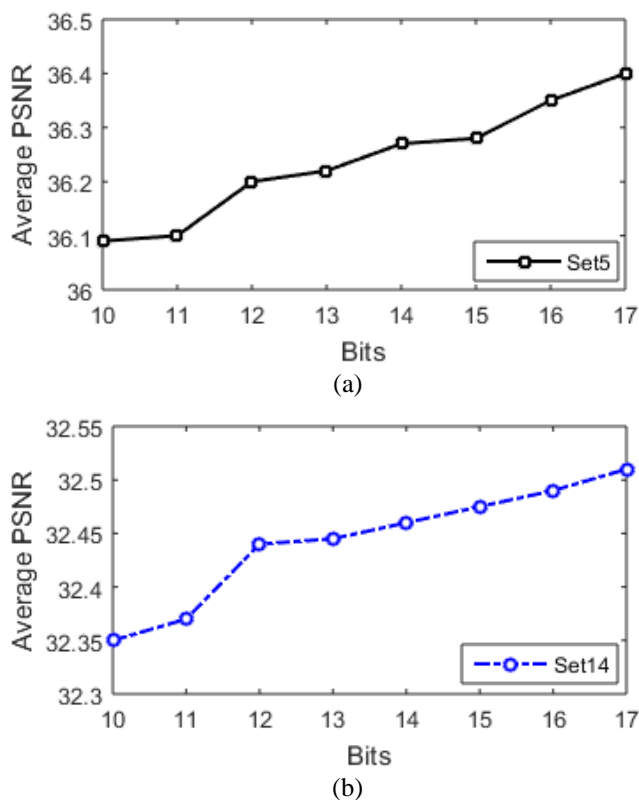


Fig.8. Average PSNR (dB) of 2X magnification with different bits depth of the LPE code, (a) on image set 'Set5', (b) on image set 'Set14'.

By increasing the bit-depth of LPE code, the performance of the proposed method can be further improved. Note that the number of training images is also required to be increased to ensure there are enough LR and HR samples in each class when the bit-depth of LPE code increases.

IV. CONCLUSIONS

In this paper we propose an effective and extendible image super-resolution framework without dictionary learning, namely local patch classification (LPC) based framework. In the proposed framework, local patches are classified into different classes by means of the proposed local patch encoding (LPE). The projection matrix of each class is then computed by utilizing a proposed constraint. In the reconstructing stage, a HR patch can be simply reconstructed by computing the LPE code of LR patch and multiplying the LR patch with corresponding projection matrix. Experimental results on several image sets demonstrate that the proposed method outperforms some state-of-the-art methods. By using the proposed framework, a lot of local pattern classification methods can be directly introduced to the SR problem. Hence, the proposed framework is open and easy to be extended.

ACKNOWLEDGEMENTS

The authors would like to sincerely thank W. S. Dong, R. Zeyde, R. Timofte, and C. Dong for sharing the source codes of the ASDS, the Zeyde's, the ANR, and the SRCNN methods.

REFERENCE

- [1] R. Keys, "Cubic convolution interpolation for digital image processing," *IEEE Trans. Acoustics, Speech Signal Process.*, vol. 29, no. 6, pp. 1153-1160, Dec. 1981.
- [2] T. M. Lehmann, C. Gonner, and K. Spitzer, "Survey: Interpolation methods in medical image processing," *IEEE Trans. Med. Imag.*, vol. 18, no. 11, pp. 1049-1075, Nov. 1999.
- [3] S. Dai, M. Han, W. Xu, Y. Wu, and Y. Gong, "Soft edge smoothness prior for alpha channel super resolution," in *Proc. IEEE Conf. Comput. Vis. Pattern Recognit.*, Jun. 2007, pp. 1-8.
- [4] X. Li and M. T. Orchard, "New edge-directed interpolation," *IEEE Trans. Image Process.*, vol. 10, no. 10, pp. 1521-1527, Oct. 2001.
- [5] F. Zhou, W. Yang, and Q. Liao, "Interpolation-based image super-resolution using multisurface fitting," *IEEE Trans. Image Process.*, vol. 21, no. 7, pp. 3312-3318, Jul. 2012.
- [6] Q. Wang and R. K. Ward, "A new orientation-adaptive interpolation method," *IEEE Trans. Image Process.*, vol. 16, no. 4, pp. 889-900, Apr. 2007.
- [7] C. Zwart and D. Frakes, "Segment Adaptive Gradient Angle Interpolation," *IEEE Trans. Image Process.*, vol. 22, no. 8, pp. 2960-2969, Aug. 2013.
- [8] X. Liu, D. Zhao, R. Xiong, S. Ma, and W. Gao, "Image interpolation via regularized local linear regression," *IEEE Trans. Image Process.*, vol. 20, no. 12, pp. 3455-3469, Dec. 2011.
- [9] Q. Wang, R. Ward, and J. Zou, "Contrast enhancement for enlarged images based on edge sharpening," in *Proc. IEEE Int. Conf. Image Process.*, Sep. 2005, vol. 2, pp. 1-4.
- [10] A. Giachetti and N. Asuni, "Real-time artifact-free image upscaling," *IEEE Trans. Image Process.*, vol. 20, no. 10, pp. 2760-2768, Oct. 2011.
- [11] X. Liu, D. Zhao, J. Zhou, W. Gao, and H. Sun, "Image Interpolation via Graph- Based Bayesian Label Propagation," *IEEE Trans. Image Process.*, vol. 23, no. 3, pp. 1084-1096, Mar. 2014.
- [12] M. Irani and S. Peleg, "Motion analysis for image enhancement: Resolution, occlusion, and transparency," *J. Vis. Commun. Image Represent.*, vol. 4, no. 4, pp. 324-355, 1993.
- [13] R. Fattal, "Image Upsampling via impose edge statistics," *ACM Trans. Graph.*, vol. 26, no. 3, Jul. 2007, Art. ID 95.
- [14] J. Sun, Z. Xu, and H. Y. Shum, "Image super-resolution using gradient profile prior," in *Proc. IEEE Conf. Comput. Vis. Pattern Recognit.*, Jun. 2008, pp. 1-8.
- [15] L. Wang, S. Xiang, G. Meng, et al, "Edge-Directed Single Image Super-Resolution via Adaptive Gradient Magnitude Self-Interpolation," *IEEE Trans. Circuits and Syst. Video Technol.*, vol. 23, no. 8, pp. 1289-1299, Aug. 2013.
- [16] H. Xu, G. Zhai, and X. Yang, "Single image super-resolution with detail enhancement based on local fractal analysis of gradient," *IEEE Trans. Circuits and Syst. Video Technol.*, vol. 23, no. 10, pp. 1740-1754, Oct. 2013.
- [17] L. Wang, H. Wu, and C. Pan, "Fast image upsampling via the displacement field," *IEEE Trans. Image Process.*, vol. 23, no. 12, pp. 5123-5135, Dec. 2014.
- [18] Q. Shan, Z. Li, J. Jia, et al, "Fast image/video upsampling," *ACM Trans. Graph.*, vol. 27, pp. 32-39, 2008.
- [19] T. Michaeli and M. Irani, "Nonparametric blind super-resolution," in *Proc. IEEE Int. Conf. Comput. Vis.*, Dec. 2013, pp. 945-952.
- [20] N. Efzrat, D. Glasner, A. Apartsin, et al., "Accurate blur models vs. image priors in single image super-resolution," in *Proc. IEEE Int. Conf. Comput. Vis.*, Dec. 2013, pp. 2832- 2839.
- [21] K. Zhang, X. Gao, D. Tao, and X. Li, "Single image super-resolution with non-local means and steering kernel regression," *IEEE Trans. Image Process.*, vol. 21, no. 11, pp. 4544-4556, Nov. 2012.
- [22] Y. Zhao, R. Wang, W. Wang, and W. Gao, "High Resolution Local Structure-Constrained Image Upsampling," *IEEE Trans. Image Process.*, vol. 24, no. 11, pp. 4394-4407, Nov. 2015.
- [23] A. Marquina, and S. J. Osher, "Image super-resolution by TV regularization and Bregman iteration," *J. Sci. Comput.*, vol. 37, no. 3, pp. 367-382, Dec. 2008.
- [24] W. T. Freeman, E. C. Pasztor, and O. T. Carmichael, "Learning low-level vision," *Int. J. Comput. Vis.*, vol. 40, no. 1, pp. 25-47, Jun. 2000.
- [25] J. Sun, N. N. Zheng, H. Tao, and H. Shum, "Image hallucination with primal sketch priors," in *Proc. IEEE Conf. Comput. Vis. Pattern Recognit.*, Jun. 2003, vol. 2, pp. 729-736.

- [26] Z. Xiong, D. Xu, X. Sun, et al., "Example-based super-resolution with soft information and decision," *IEEE Trans. Multimedia*, vol. 15, no. 6, pp. 1458-1465, 2013.
- [27] H. Chang, D. Y. Yeung, and Y. Xiong, "Super-resolution through neighbor embedding," in *Proc. IEEE Conf. Comput. Vis. Pattern Recognit.*, Jun. 2004, vol. 1, pp. 275-282.
- [28] M. Bevilacqua, A. Roumy, et al., "Low-complexity single image super-resolution based on nonnegative neighbor embedding," in *Proc. British Machine Vis. Conf.*, 2012, pp.1-10.
- [29] Y. Zhao, R. Wang, W. Wang, W. Gao, "Multilevel modified finite radon transform network for image upsampling," *IEEE Trans. Circuits and Syst. Video Technol.*, vol.26, no.12, pp.2189-2199, Dec. 2016.
- [30] J. Yang, J. Wright, T. S. Huang, and Y. Ma, "Image super-resolution via sparse representation," *IEEE Trans. Image Process.*, vol. 19, no. 11, pp. 2861-2873, Nov. 2010.
- [31] J. Yang, Z. Wang, Z. Lin, X. Shu, and T. Huang, "Bilevel sparse coding for coupled feature spaces," in *Proc. IEEE Conf. Comput. Vis. Pattern Recognit.*, Jun. 2012, pp. 2360-2367.
- [32] W. Dong, D. Zhang, G. Shi, et al. "Image deblurring and super-resolution by adaptive sparse domain selection and adaptive regularization," *IEEE Trans. Image Process.*, vol. 20, no. 7, pp. 1838-1857, Jul. 2011.
- [33] L. He, H. Qi, and R. Zaretzki, "Beta Process Joint Dictionary Learning for Coupled Feature Spaces with Application to Single Image Super-Resolution," in *Proc. IEEE Conf. Comput. Vis. Pattern Recognit.*, Jun. 2013, pp. 345 - 352.
- [34] T. Peleg and M. Elad, "A statistical prediction model based on sparse representations for single image super-resolution," *IEEE Trans. Image Process.*, vol.23, no. 6, pp. 2569-2581, Jun. 2014.
- [35] W. Dong, L. Zhang, G. Shi, and X. Li, "Nonlocally centralized sparse representation for image restoration," *IEEE Trans. Image Process.*, vol. 22, no. 4, pp. 1620-1630, Apr. 2013.
- [36] R. Zeyde, M. Elad, and M. Protter, "On single image scale-up using sparse-representations," *Curv. Surfaces*, pp. 711- 730, 2010
- [37] J. Liu, W. Yang, X. Zhang and Z. Guo, "Retrieval Compensated Group Structured Sparsity for Image Super-Resolution," *IEEE Trans. Multimedia*, vol. 19, no. 2, pp. 302-316, Feb. 2017.
- [38] Z. Zhu, F. Guo, H. Yu, et al., "Fast single image super-resolution via self-example learning and sparse representation," *IEEE Trans. Multimedia*, vol. 16, no. 8, pp. 2178-2190, 2014.
- [39] D. Glasner, S. Bagon, and M. Irani, "Super-resolution from a single image," in *Proc. IEEE Int. Conf. Comput. Vis.*, Sep. 2009, pp. 349-356.
- [40] G. Freedman, R. Fattal, "Image and video upscaling from local self-examples," *ACM Trans. Graph.*, vol. 30, no. 2, pp. 12-23, 2011.
- [41] K. Zhang, X. Gao, D. Tao, and X. Li, "Single image super-resolution with multiscale similarity learning," *IEEE Trans. Neural Netw. Learn. Syst.*, vol. 24, no. 10, pp. 1648-1659, Oct. 2013.
- [42] J. Yang, Z. Lin, S. Cohen, "Fast image super-resolution based on in-place example regression," in *Proc. IEEE Conf. Comput. Vis. Pattern Recognit.*, Jun. 2013, pp. 1059-1066.
- [43] M. Yang, and Y. Wang, "A self-learning approach to single image super-resolution," *IEEE Trans. Multimedia*, vol. 15, no.3, pp. 498-508, 2013.
- [44] R. Timofte, V. D. Smet, and L. V. Gool, "Anchored neighborhood regression for fast example-based super-resolution," in *Proc. IEEE Int. Conf. Comput. Vis.*, Dec. 2013, pp. 1920- 1927.
- [45] R. Timofte, V. D. Smet, and L. V. Gool, "A+: Adjusted anchored neighborhood regression for fast super-resolution," *Asian Conf. Comput. Vis.*, Nov. 2014, pp. 1-15.
- [46] K. Zhang, D. Tao, X. Gao, X. Li, and Z. Xiong, "Learning multiple linear mappings for efficient single image super-resolution," *IEEE Trans. Image Process.*, vol. 24, no. 3, pp. 846-861, Mar. 2015.
- [47] J. Jiang, X. Ma, C. Chen, et al., "Single Image Super-Resolution via Locally Regularized Anchored Neighborhood Regression and Nonlocal Means," *IEEE Trans. Multimedia*, vol. 19, no. 1, pp. 15-26, 2017.
- [48] W. Yang, Y. Tian, F. Zhou, et al., "Consistent Coding Scheme for Single-Image Super-Resolution Via Independent Dictionaries," *IEEE Trans. Multimedia*, vol. 18, no. 3, pp. 313-325, 2016.
- [49] Y. Zhang, Y. Zhang, J. Zhang, et al., "CCR: Clustering and Collaborative Representation for Fast Single Image Super-Resolution," *IEEE Trans. Multimedia*, vol. 18, no. 3, pp. 405-417, 2016.
- [50] S. Schuler, C. Leistner, H. Bischof, "Fast and accurate image upscaling with super-resolution forests," in *Proc. IEEE Conf. Comput. Vis. Pattern Recognit.*, 2015, pp.3791-3799.
- [51] N. Kumar, and A. Sethi, "Fast Learning-Based Single Image Super-Resolution," *IEEE Trans. Multimedia*, vol.18, no.8, pp.1504-1515, 2016.
- [52] C. Dong, C. Loy, K. He, and X. Tang, "Image super-resolution using deep convolutional networks," *IEEE Trans. Pattern Anal. Mach. Intell.*, vol. 38, no. 2, pp. 295-307, Jul. 2016.
- [53] J. Kim, J. Lee, and K. Lee, "Accurate image super-resolution using very deep convolutional networks," in *Proc. IEEE Conf. Comput. Vis. Pattern Recognit.*, Jun. 2016, vol. 1, pp. 1646-1654.
- [54] Z. Cui, Z. H. Chang, S. Shan, et al., "Deep network cascade for image super-resolution," in *Proc. Euro. Conf. Comput. Vis.*, 2014, pp.49-64.
- [55] W. Shi, J. Caballer, F. Huszar, et al., "Real-Time Single Image and Video Super-Resolution Using an Efficient Sub-Pixel Convolutional Neural Network," in *Proc. IEEE Conf. Comput. Vis. Pattern Recognit.*, Jun. 2016, vol. 1, pp. 1874-1883.
- [56] Y. Huang, W. Wang, L. Wang, "Bidirectional recurrent convolutional networks for multi-frame super-resolution," in *Proc. Conf. Neural Inform. Process. Syst.*, Dec. 2015, pp. 235-243.
- [57] D. Martin, C. Fowlkes, D. Tal, et al., "A database of human segmented natural images and its application to evaluating segmentation algorithms and measuring ecological statistics," in *Proc. IEEE Int. Conf. Comput. Vis.*, 2001, pp. 416-423.
- [58] N. Wang, D. Tao, X. Gao, X. Li, and J. Li, "A comprehensive survey to face hallucination," *Int. J. Comput. Vis.*, vol. 106, no. 1, pp. 9-30, Jan. 2014.
- [59] T. Ojala, M. Pietikainen, and T. Maenpaa, "Multiresolution gray-scale and rotation invariant texture classification with local binary patterns," *IEEE Trans. Pattern Anal. Mach. Intell.*, vol. 24, no. 7, pp. 971-987, Jul. 2002.
- [60] Z. H. Guo, D. Zhang, and D. Zhang, "A completed modeling of local binary pattern operator for texture classification," *IEEE Trans. Image Process.*, vol. 19, no. 6, pp. 1657-1663, Jun. 2010.
- [61] Y. Zhao, D. Huang, W. Jia, "Completed local binary count for rotation invariant texture classification", *IEEE trans. Image Process.*, vol.21, pp. 4492-4497, Oct. 2012.
- [62] Z. Wang, A. Bovik, H. Sheikh, et al., "Image quality assessment: from error visibility to structural similarity," *IEEE Trans. Image Process.*, vol. 13, no. 4, pp. 600-612, 2004.
- [63] C. Yang, C. Ma, M. Yang, "Single-image super-resolution: a benchmark," in *Proc. Euro. Conf. Comput. Vis.*, Sep. 2014, pp. 372-386.
- [64] H. Sheikh, A. Bovik, G. De Veciana, "An information fidelity criterion for image quality assessment using natural scene statistics," *IEEE Trans. Image Process.*, vol. 14, no. 12, pp. 2117-2128, 2005.